Investigation of the Affinity of Aptamers for Bacteria by Surface Plasmon Resonance Imaging Using Nanosomes

Mathilde Manceau, Carole Farre, Florence Lagarde, Raphaël Mathey, Arnaud Buhot, Jasmina Vidic, Vincent Léguillier, Yanxia Hou, Carole Chaix

Investigation of the Affinity of Aptamers for Bacteria by Surface Plasmon Resonance Imaging using Nanosomes

Mathilde MANCEAU,[†] Carole FARRE,[†] Florence LAGARDE,[†] Raphaël MATHEY,[§] Arnaud BUHOT,[§] Jasmina VIDIC,[#] Vincent LÉGUILLIER,[#] Yanxia HOU,[§] Carole CHAIX[†*]*

[†]*Univ. Claude Bernard Lyon1, CNRS, ISA, UMR5280, 69100 Villeurbanne, France*

[§]*Univ. Grenoble Alpes, CEA, CNRS, Grenoble INP, IRIG, SyMMES, 38000 Grenoble, France*

[#]*Univ. Paris-Saclay, INRAE, AgroParisTech, UMR 1319, Micalis Institute, 78350 Jouy-en-Josas, France*

*Corresponding authors: carole.chaix-bauvais@univ-lyon1.fr; mathilde.manceau@isa-lyon.fr

KEYWORDS: Aptamer, *Bacillus cereus*, bacteria, Surface Plasmon Resonance, membrane vesicle, affinity

ABSTRACT

The cell-SELEX method enables efficient selection of aptamers that bind whole bacterial cells. However, after selection, it is difficult to determine their binding affinities using common screening methods because of the large size of the bacteria. Here we propose a simple surface plasmon resonance imaging method (SPRi) for aptamer characterization using bacterial membrane vesicles, called nanosomes, instead of whole cells. Nanosomes were obtained from membrane fragments after mechanical cell disruption in order to preserve the external surface epitopes of the bacterium used for their production. The study was conducted on *Bacillus cereus (B. cereus),* a gram-positive bacterium commonly found in soil, rice, vegetables and dairy products. Four aptamers and one negative control were initially grafted onto a biochip. The binding of *B. cereus* cells and nanosomes to immobilized aptamers was then compared. The use of nanosomes instead of cells provided a 30-fold amplification of the SPRi signal, thus allowing the selection of aptamers with higher affinities. Aptamer SP15 was found to be the most sensitive and selective for *B. cereus* ATCC14579 nanosomes. It was then truncated into three new sequences (SP15M, SP15S1 and SP15S2) to reduce its size while preserving the binding site. Fitting the results of the SPRi signal for *B. cereus* nanosomes showed a similar trend for SP15 and SP15M, and a slightly higher apparent association rate constant k_{on} for SP15S2, which is the truncation with a high probability of a G-quadruplex structure. These observations were confirmed on nanosomes from *B. cereus* ATCC14579 grown in milk and from the clinical strain *B. cereus* J066. The developed method was validated using fluorescence microscopy on whole *B. cereus* cells and the SP15M aptamer labelled with a rhodamine. This study showed that nanosomes can successfully mimic the bacterial membrane with great potential for facilitating the screening of specific ligands for bacteria.

INTRODUCTION

The development of biosensors has grown steadily in recent years from the detection of small molecules to living organisms, such as bacteria. Bioreceptors are key elements in biosensor development as they enable recognition of the target. Among the available bioreceptors, aptamers are attracting increasing interest because of their low cost, high chemical stability and resistance.[1] The single-stranded nucleic acid sequences are generally selected by Systematic Evolution of Ligands by Exponential Enrichment (SELEX). After several rounds, this technique yields a range of potential candidates that must be further characterized to determine their binding affinities and specificities. It is also often necessary to perfect their performance by truncating the selected aptamers, and then ensuring that the latter maintain a stable conformation in complex matrices when grafted onto a substrate.[2] Various techniques can be used to characterize the affinity and specificity of aptamers.[3] However, when SELEX is applied to cells like bacteria (cell-SELEX), most of these affinity characterization methods are actually unsuitable, primarily due to the large size of bacteria. The most commonly used methods are fluorescence spectrophotometry and flow cytometry,[2] but both require a fluorescent label and cannot be used for multiplexed analyses.

In this context, label-free optical techniques, such as surface plasmon resonance (SPR), are of particular interest. Among SPR methods, SPR imaging (SPRi) allows the multiplexing of analyses and direct comparison of the interactions between different bioreceptors with the same analyte when coupled to a microarray. However, one of its limitations is a low detection sensitivity for large bio-analytes, such as bacteria, mainly due to the low-range penetration of the plasmonic waves – within 200nm of the prism surface.[4] The average size of a bacterium is a few micrometers. Consequently, at the micrometer scale, most the bacterial cell volume immobilized on the chip is outside the sensing range in the standard SPRi configuration. Additionally, it is worth mentioning that the refractive index of bacteria can vary from 1.36-1.40,[5] which is very close to the value of water (1.33). The SPR measurement is made less sensitive by the small variation in the refractive index between the bacteria and the aqueous medium.

Several SPR-derived methods have therefore been developed to improve the sensitivity of SPR for detecting bacteria. These include long-range SPR, which extends the evanescent field of the surface plasmon,[6] and localized surface plasmon methods, which use nanoparticles to enhance the oscillation of the surface plasmon.[7] SPR sensitivity can also be enhanced using the capture/culture/measure process, which improves sensitivity by culturing captured bacteria directly on the prism.[8] However, these techniques require either special technical equipment or significant analysis time, therefore a new approach would be desirable.

SPR is known to be highly sensitive to the interaction of liposome-like vesicles with a gold surface.[9,10] Furthermore, bacteria naturally secrete external membrane vesicles ranging from 20 to 400nm in diameter.[11] These are formed when a portion of the bacterial membrane protrudes and buds off under different vesiculation mechanisms, entrapping various bio-components.[12] Inspired by this phenomenon, nanometer-sized vesicles (called nanosomes) have been developed to enable bacterial detection by SPRi with improved sensitivity. In the literature, Elie-Caille et al. describe the production of proteoliposomes that include native mitochondrial membrane proteins from human hepatic cells.[13] Similar strategies have also been applied to yeast,[14] but to our knowledge, never to bacteria. In our protocol, nanosomes were formed by mechanical cell disruption and membrane fraction purification. Bacterial nanosomes offer the advantages of being able to manipulate pathogenic strains easily and store them for long periods without degradation.

This study was conducted on *Bacillus cereus* and its respective aptamers. *B. cereus* is a gram-positive, rod-shaped, spore-forming bacterium, commonly found in soil, air, rice, vegetables and dairy products.[15] Within the *B. cereus* group, *B. cereus sensu stricto* (*B. cereus s. s.*) is one of the major causes of food poisoning in Europe, along with the *Staphylococcus aureus* and *Clostridium perfringens* bacteria.[16,17] *B. cereus s. s.* poisoning is associated with the production of the emetis-inducing toxin cereulide or diarrhea-inducing enterotoxins.

Several aptamer sequences targeting *B. cereus* cells have been reported. Two of these studies selected aptamers using cell-SELEX,[18,19] while the other study provides little information on how

the sequence was selected.[20] However, the affinities of these aptamers cannot be compared based on the information in these publications. Although the affinity constants in both studies by Zhou et al. and Wang et al. between their aptamers and *B. cereus* were calculated by flow cytometry, the conditions under which the experiments were performed were different, making comparison impossible.[18,19] Furthermore, most of the sequences described are long (around 80-mers), which constitutes an obstacle to efficient grafting onto a substrate while conserving their structures. Moreover, it is expensive to synthesize long sequences and the yield is generally less than with shorter ones.

In this context, the affinities of described aptamers were compared by SPRi using nanosomes. The aptamer exhibiting the highest affinity and specificity toward *B. cereus* ATCC14579 nanosomes was then truncated at various sites and affinity toward nanosomes produced from *B. cereus* ATCC14579 grown in milk and the clinical strain *B. cereus* J066 was also studied. Finally, the truncated aptamer with the highest affinity and specificity to *B. cereus* nanosomes was modified with a fluorescent probe at the 5' end. Its interaction with the whole *B. cereus* bacterial cells was investigated and confirmed by fluorescence microscopy to validate the proposed screening method.

MATERIALS AND METHODS

Chemicals. Monobasic and dibasic sodium phosphate, 2-amino-2-(hydroxymethyl)-1,3-propanediol (TRIS), phenylmethanesulfonylfluoride (PMSF), ethylenediaminetetraacetic acid (EDTA), sodium chloride, magnesium chloride hexahydrate, ethanolamine, HPLC grade ethanol, agar, Bovine Serum Albumin (BSA) and glycerol were all purchased from Sigma-Aldrich. Sodium hydroxide and potassium chloride were from VWR chemicals and Prolabo, respectively, and HS-C_{11}-$(EG)_6$-OCH_2-COONHS (PEG-NHS) was purchased from ProChimia Surfaces (Gdynia). Brain Heart Infusion (BHI) was purchased from Fluka Analytical. Scream milk powder was purchased in local supermarket (Auchan, France). The complete proteases inhibitor cocktail was purchased from Roche (Sigma, France). Aptamers and ZIP9 were ordered from Eurogentec (Belgium).

Bacterial strains of *B. cereus* ATCC14579, *Bacillus subtilis* BSB1 and *Escherichia coli* K12 were from the INRAE lab collection. Clinical strain *B. cereus* J066 was a kind gift from Dr Virginie Rigourd (Région Île-de-France Human Milk Bank, Hôpital Necker-Enfants Malades).

Design of aptamer sequences. A bibliographic study on specific aptamers for *B. cereus* helped us to select four sequences described as having strong affinity for the bacterial strain. Two aptamer sequences, called SP15 and SP16,[18] were retained from Wang et al.'s patent. The recent study by Zhou et al. used a short aptamer truncation sensitive to *B. cereus* in a biosensor, referred to as a capture aptamer, which we abbreviated as Cap_apt.[19] Finally, Zheng et al. used an anti-*B. cereus* aptamer, which we called Apt_Bc.[20] A 5' amine modification and a polythymidine ($p(T)_{10}$) spacer were added to each aptamer to allow efficient aptamer grafting and respective structuration on a functionalized surface. The secondary structures of the aptamers were predicted using the UNAFold web server.[21] Medium and short truncations were made on the SP15 aptamer. The truncations were designed by selecting the most likely structuration sites (loop and G-quadruplex regions) and the most favorable thermodynamics. Table 1 summarizes the selected sequences, their length, and the estimated melting temperature of their folded structure (T_m).

Table 1. Sequences of ssDNA aptamers and ZIP9 oligonucleotide as negative control used in this study

Name	Sequence (5' → 3')	Length	T_m
SP15	NH_2-C_6-$p(T)_{10}$-AGC AGC ACA GAG GTC AGA TGG GCG GGT TTG GAT CTT TGG TTG GCG CCT GTT TCT TTA TGA CCT ATG CGT GCT	82 nt	60 °C
SP15M	NH_2-C_6-$p(T)_{10}$-AGG TCA GAT GGG CGG GTT TGG ATC TTT GGT TGG CGC CTG TTT CTT TAT GAC CT	63 nt	63.5 °C
SP15S1	NH_2-C_6-$p(T)_{10}$-GGC GGG TTT GGA TCT TTG GTT GGC GCC	37 nt	59.9 °C
SP15S2	NH_2-C_6-$p(T)_{10}$-GGT CAG ATG GGC GGG TTT GGA TCT TTG GTT GG	42 nt	NA
SP16	NH_2-C_6-$p(T)_{10}$-AGC AGC ACA GAG GTC AGA TGA TAT GTT TAC GCC AGT GGT ATT ATT GGG GTT GAT ATG TCA CCT ATG CGT GCT	82 nt	44.8 °C
Cap_apt	NH_2-C_6-$p(T)_{10}$-ATG GGC TAC TGG AGC ATC TGT TTT TAT GGG CTA CTG GAG CAT CTG	55 nt	50.2 °C
Apt_Bc	NH_2-C_6-$p(T)_{10}$-AGC AGC ACA GAG GTC AGA TGC CCC CCT TTT ATC CGT CGG CAT GAT GTC TCC CGA TCC GGT CCT ATG CGT GCT A	83 nt	47.2 °C
ZIP9	NH_2-C_6-$p(T)_5$-GAC CAT CGT GCG GGT AGG TAG ACC	29 nt	NA

***B. cereus* culture and quantification.** Prior to each experiment, bacteria were grown on BHI agar plates overnight at 37 °C and resuspended in 10 mL running buffer (TRIS 50 mM, NaCl 100 mM, KCl 5 mM, $MgCl_2$ 1 mM, pH=7.4). The suspension was adjusted to OD_{600} = 1.5 and dilutions (10^8 to 10^1 CFU/mL) were prepared. Quantitative bacterial enumeration was performed by plating 100 µL aliquots of the dilutions (10^4 to 10^2 CFU/mL) on BHI agar plates in duplicate to confirm bacterial concentration.

Preparation of nanosomes. To produce nanosomes, bacterial cells were grown in BHI medium overnight. For test on milk-adapted *B. cereus*, cells grown in BHI were incubated in 1% milk (1g of milk powder in 100 mL) for 2 hrs before nanosome production. Bacterial cells were collected by centrifugation (5 min at 4000 g), washed two times with ice-cold water and resuspended in an equal volume of ice-cold lysis buffer (50 mM Tris-HCl, pH 7.5, 1 mM EDTA, 0.1 mM PMSF and the complete protease inhibitor cocktail). The suspension was sonicated to break bacterial cells, and then centrifuged at 10,000*g*, at 4 °C for 30 min to remove unbroken cells and cell debris. Subsequently, the supernatant was ultracentrifuged at 40,000 g at 4 °C for 40 min. Obtained pellet, enriched in membrane fractions, was resuspended in the lysis buffer supplemented with 10% (w/w) glycerol with a Dounce homogenizer, and stored in aliquots at −70 °C. The protein concentration of the membrane preparation was determined using the copper-based BCA reagent (Pierce, France) and BSA as a standard. Before use, the nanosomes were redispersed by sonication for 30 min in ice-cold water (Tanssonic sonicator, Prolabo).

Physicochemical characterization of nanosomes. Dynamic Light Scattering (DLS) was carried out with a Zetasizer instrument (Malvern Panalytical, France) to determine the hydrodynamic diameter of nanosomes. A disposable cuvette ZEN0040 was filled with 200 µL of nanosome suspensions in running buffer (1:1000). Measurements in triplicate were achieved at room temperature after an equilibration time of 120 s. The material and dispersant refractive indexes were 1.45 and 1.33, respectively.

Nanoparticle Tracking Analysis (NTA, NS300, Malvern Panalytical, France) was used to determine the size distribution and concentration of nanosomes. The sample dilutions were made in the running buffer to obtain between 20 and 70 nanosomes per frame. Three 1 min videos were recorded at room temperature for each sample with a camera level of 14. The analysis was performed with the NanoSight NTA 3.4.4 software by choosing a detection threshold of 7.

Transmission electron microscopy (TEM) was performed on a JEOL 1400 flash instrument operating at an acceleration voltage of 120 kV (Centre Technologique des Microstructures, Lyon, France). Nanosomes were observed after deposition of 3 µL of diluted suspension on a formvar-carbon-coated copper grid and evaporation to dryness. They were stained on the droplet of 1% uranyl acetate solution for 30 s at room temperature and rinsed twice with distilled water.

Raman spectra were acquired using a confocal Raman microscope (LabRAM HR Evolution spectrometer (HORIBA) equipped with a CCD detector). The exciting line at 532 nm was focused on the sample with a 100x objective. The power of the incident beam on the sample was about 2 mW, the spectral resolution was about 4 cm^{-1}. Prior to analysis, 5 µL of nanosomes from *B. cereus* grown in BHI diluted in 0.9% w/v NaCl solution in water was deposited on a calcium fluoride slide and allowed to air dry.

Preparation of SPRi chips. The prisms were treated by plasma (0.6 mbar, 75% oxygen, 25% argon, 80% power, 3 min, Femto, Diener electronic GmbH + Co. KG, Germany) and then directly immersed in 3mL of 1 mM PEG-NHS solution in ethanol (HPLC grade) overnight at room temperature. The next day, the prisms were rinsed twice in ethanol (HPLC grade) baths and dried under air flow prior to spotting the aptamers, ZIP9 and blank solutions. 20 µL solutions of 15 µM aptamers (SP15S1, SP15S2, SP15M, SP15, SP16, Apt_Bc and Cap_apt) and 20 µL of 15 µM ZIP9 oligonucleotide in grafting buffer (94 mM Na_2HPO_4, 6 mM NaH_2PO_4, 100 mM NaCl, 10 % glycerol, pH=8.0) were prepared. A thermal shock (1 min at 95°C followed by 10 min in ice) was applied to the aptamer solutions to unfold the aptamers. Aptamer unfolding is necessary to make the primary amine of the aptamers accessible and then facilitate their grafting onto the prism. Using

a sciFLEXARRAYER electronic robot spotter (Scienion), a 6 nL drop of each aptamer sample was deposited in five replicates placed randomly on the prism. After spotting, the prisms were left for 2 hours in a humidity-controlled chamber at 25°C for grafting. Then, the prisms were rinsed twice in cleaning buffer (94 mM Na_2HPO_4, 6 mM NaH_2PO_4, 100 mM NaCl, pH=8.0) and immersed in 10 mL ethanolamine (1 mM in cleaning buffer) to block any NHS sites that had not reacted. Finally, the prisms were rinsed twice in running buffer and stored at 4 °C in 10 mL running buffer.

SPRi setup. The SPRi experiments were performed using an SPRi-Lab+ instrument (Horiba Scientific, France) placed inside a thermal chamber at 25 °C. A polarized 680nm laser beam was reflected by a mirror to hit the prism (Horiba Scientific) at the chosen working angle. The regions of interest (ROI) corresponding to the aptamer spots were selected using commercial software. The reflected intensity changes at the ROI were monitored by a CCD camera. The injector was made of a 6-port valve with a 500 µL loop. Samples were injected into a microfluidic cuvette at the top of the microarray via inlet tubing. The flow was controlled by a 2.5 mL syringe pump (Cavro) and degassed in-line (Elite degassing system, Alltech).

SPRi measurement. Before each experiment, the prism was cleaned by immersing it twice for five seconds in 150 mL ultrapure water. It was then mounted on the SPRi apparatus, and the signal was stabilized under a 50 µL/min flow of running buffer before selecting the ROI. The working angle was selected as being the maximum derivative of the plasmon curve. This is where the differences in reflectivity are the most sensitive. Each analysis began with the injection of 1 M NaCl at 250 µL/min for 2 min. Once the signal was stable, the flow rate was set at 50 µL/min and BSA 1% (w/v) in running buffer was injected for 8 min. Then, nanosomes were injected for 25 min at 15.6 µL/min. Because of the high bacteria concentrations used, bacteria were injected for 1 min at 250 µL/min to reduce the measurement dead time, followed by 14 min at 15.6 µL/min. All the SPRi experiments were performed under dynamic flow. The nanosome and bacteria injections were followed by a 25 min washing step with running buffer until the signal was stabilized. The prism

was regenerated by injecting 10 mM NaOH solution in ultrapure water for 8 min. Figure 1 represents the SPRi system and the strategy used in this study.

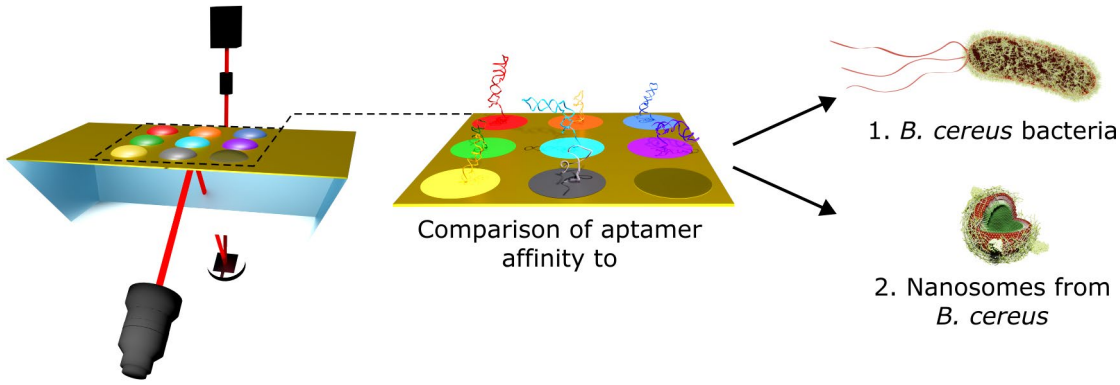

Figure 1. Schematic representation of the biochip functionalized with different aptamers and used to compare their affinity toward *B. cereus* bacteria and nanosomes from *B. cereus* by SPRi.

Optical imaging of *B. cereus* bacteria bound with the fluorescence-labeled SP15M aptamer. SP15M aptamer labeled with a rhodamine tag at the 5' end (Rhod-SP15M) was ordered from Eurogentec. 100 µL of Rhod-SP15M aptamer (500 nM, running buffer) was incubated with 100 µL of *B. cereus* (5 x 10^7 CFU/mL, running buffer) at 25 °C for 45 minutes with gentle shaking (300rpm). After incubation, the suspension was centrifuged (2,000 rpm, 1 min) and the supernatant containing unbound aptamers was removed. The pellet was resuspended in running buffer to obtain a volume of 200 µL and the suspension was centrifuged a second time (2,000 rpm, 1 min). The pellet was suspended once again in running buffer to obtain a final volume of 100 µL. 10 µL of this suspension was dropped onto a poly-L-lysine coated slide (P0425, Merck) for 20 min. The slide was then examined by white light and fluorescence reflection microscopy using a Zeiss Axioplan 2 imaging device (Zeiss, Germany). Photos were taken with a coverslip and using a 40x/0.45 lens. Fluorescence images were taken after excitation at a wavelength of 525 nm. Non-specificity was assessed by repeating this protocol using the ZIP9 oligonucleotide as a negative control (Rhod-ZIP9).

RESULTS AND DISCUSSION

Preparation and characterization of bacterial nanosomes. The originality of this work lies in the development of nanosomes to replace bacterial cells for improved SPRi sensitivity. Our objective was to obtain nano-sized vesicles with an external surface similar to that of whole bacteria. Nanosomes are spherical fragments of the bacterial membrane obtained by mechanical disruption. A sonication of a bacterial suspension breaks the phospholipid membranes to form fragments, which spontaneously reassemble to form nano-sized vesicles. Subsequent sonication of the preparation results in uniform vesicle sizes.[22] This simple protocol was applied to *B. cereus*, *B. subtilis* and *E. coli* bacteria. The resulting nanosomes were characterized by DLS and NTA (Table 2). According to the DLS results, the nanosomes from *B. cereus* and *B. subtilis* had an average size of approximately 300 nm with a polydispersity index below 0.3, indicating a homogeneous population of vesicles.[23] Nanosomes from *E. coli* had a smaller average size of 167.4 ± 3.9 nm with a polydispersity index of 0.40, indicating a wider size dispersion. A different trend in size was obtained by NTA, where nanosomes from *B. cereus*, *B. subtilis* and *E. coli* had an average size of about 150 nm. The difference in nanosome size obtained by NTA or DLS can be easily explained by the difference in measurement principle. DLS measures particle size according to changes in the scattered intensity of particles in suspension. In a sample containing both small and large particles, small particles will hardly be visualized and the average size will be overestimated.[24] In contrast, NTA is appropriate for a polydisperse sample because it tracks the Brownian motion of each particle in the suspension.[25] The nanosome concentration was obtained by NTA with settings optimized for quantification of *B. cereus* nanosomes. The samples were diluted in running buffer and adjusted to obtain between 20 and 70 nanosomes per frame.

The epitopes involved in aptamer-bacteria interactions are often proteins.[26] In particular, the capture aptamer in the study by Zhou et al. was shown to target amino acids in the α-helix of the *B. cereus* epiprotein.[19] For this reason, we decided to use nanosome suspensions with a constant protein concentration to compare the affinity of the aptamers with the study's different nanosomes.

This was determined by copper-based colorimetric detection, which is less affected by differences in protein composition than a Bradford assay. Protein concentrations in the bulk samples before dilution were: 1.0, 0.45 and 1.7 mg/mL for *B. cereus*, *B. subtilis* and *E. coli* nanosomes respectively.

Table 2. Nanosome characterizations. The mean hydrodynamic diameters and concentrations are given as mean values ± standard error of three replicates.

Nanosomes	d^{a}_{DLS} (nm)	PdI[b]	d_{NTA} (nm)	SE[c] (nm)	C_n[d] (particle/mL)	C_p[e] (µg/mL)
B. cereus	318.7 ± 9.4	0.27	148.0 ± 0.8	41.9 ± 1.1	$(1.18 \pm 0.02) \times 10^{11}$	80
B. subtilis	278.0 ± 2.6	0.28	164.4 ± 2.1	61.4 ± 2.0	$(5.14 \pm 0.18) \times 10^{12}$	80
E. coli	167.4 ± 3.9	0.40	142.0 ± 1.0	49.0 ± 1.8	$(1.04 \pm 0.02) \times 10^{9}$	80

[a] Mean hydrodynamic diameter, [b] Polydispersity index, [c] Standard error, [d] Concentration of nanosomes, [e] Concentration of proteins

Two Raman spectra were obtained for nanosomes from *B. cereus* in the spectral ranges of 440-4,000 cm^{-1} and 500-2,000 cm^{-1} (Figure S1, Table S1). The spectra showed characteristic Raman bands of proteins, such as protein backbone bands at 854 and 932 cm^{-1}, and amino acid bands with the characteristic phenylalanine band at 1,003 cm^{-1}. The presence of lipids was highlighted by peaks corresponding to triacylglycerol (2,935 cm^{-1}) and C-C stretch (1,127 cm^{-1}). The peaks at 1,321 and 1,340 cm^{-1} were assigned to glycosaminoglycans. Unfortunately, the analysis of a standard peptidoglycan sample purified from *B. subtilis* did not reveal any distinctive peaks compared with those already observed in the proteins. Therefore, the presence of peptidoglycan in the *B. cereus* nanosome sample could not be evaluated.

The three types of nanosomes were observed directly by TEM using negative staining with uranyl acetate (Figure 2). The nanosomes appeared as nanovesicles with a broad size distribution ranging from 100 nm to 500 nm (Figure S2). The fact that we can observe nanosomes without having to use a more adapted method, such as cryo-TEM, supports the hypothesis that nanosomes are protected by a membrane-like bacteria envelope. The negative staining induced a visible difference between the nanosomes. While nanosomes from *B. cereus* and *B. subtilis* appeared as round vesicles (Figure 2A-B), with the dye concentrated at the edges of the membrane, nanosomes from *E. coli* appeared more irregular and fragile (Figure 2C). The structures were less spherical, the

membrane fragments visible, and the dye was dispersed in different layers. This difference between nanosome structures may be related to the difference between gram-positive and gram-negative bacteria. Gram-positive bacteria are known to have a thick layer of peptidoglycan on the surface of a phospholipid membrane, while gram-negative bacteria have a thin layer of peptidoglycan sandwiched between two phospholipid layers. The picture in Figure 2C appears to show the double thickness of the phospholipid membrane of the *E coli* nanosome. The structure of nanosomes observed by microscopy thus reflects differences between the envelopes of gram-positive and gram-negative bacteria.

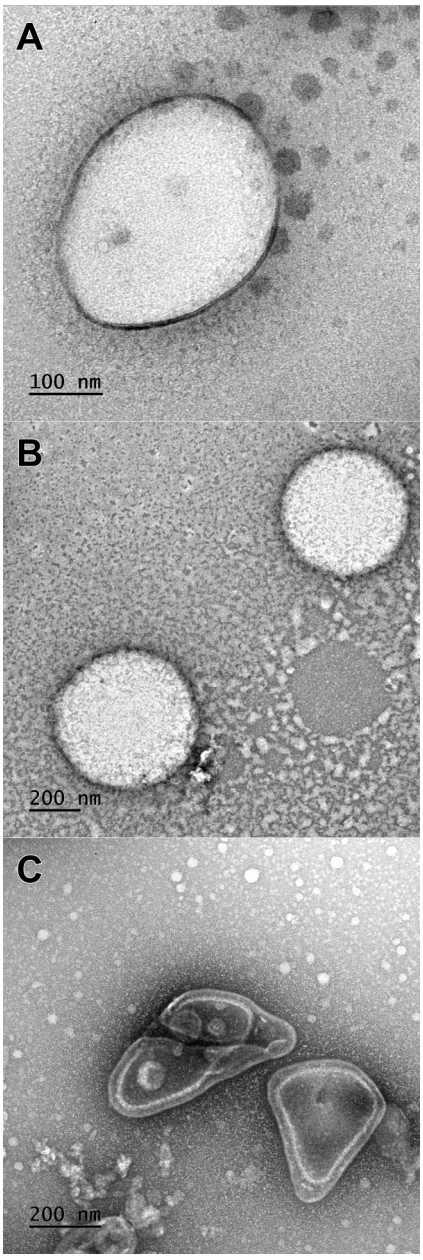

Figure 2. Transmission electron microscope images of negative stained nanosomes from (A) *B. cereus*, (B) *B. subtilis* and (C) *E. coli* bacteria.

Binding of aptamers toward *B. cereus* nanosomes. Due to its multiplexing capability, the SPRi technique was chosen to enable easy comparison of the binding capacities of four anti-*B. cereus* aptamers: SP15, SP16, Apt_Bc and Cap_apt (Table 1).[18–20] The gold-coated prisms were functionalized overnight with a thiolated PEG-NHS solution to form a self-assembled monolayer. This reagent effectively reduces non-specific interactions that may occur with bacterial samples.[27] Five replicates of each aptamer were then grafted by spotting onto the SPRi prism. A 5'amino-polythymidine ($p(T)_{10}$) was added to the aptamer sequences to serve as a spacer for efficient grafting onto the PEG-NHS-functionalized surface.[28] SPRi experiments were performed by injecting either *B. cereus* nanosomes with a protein content of 80 µg/mL or *B. cereus* bacteria at a concentration of 3.6 x 10^8 CFU/mL. Negligible changes in responses were observed during injection of the concentrated *B. cereus* bacterial suspension, while a 30-fold signal increase was obtained during injection of *B. cereus* nanosomes (Figure 3). The two trends are similar and show that SP15 and Apt_Bc have better binding magnitude toward *B. cereus* than the aptamers SP16 and Cap_apt. However, while the high standard error and low signal-to-noise ratio present in the analysis of *B. cereus* cells made aptamer discrimination difficult (Figure 3B), the use of nanosomes validated these observations with precision. The improved sensitivity actually increased the signal-to-noise ratio and decreased the standard error (Figure 3A). Cumulative injections of nanosome suspensions at different concentrations were made to perform an affinity study. However, no kinetic constants were calculated due to the low binding observed for Cap_apt and SP16 (Figure S3).

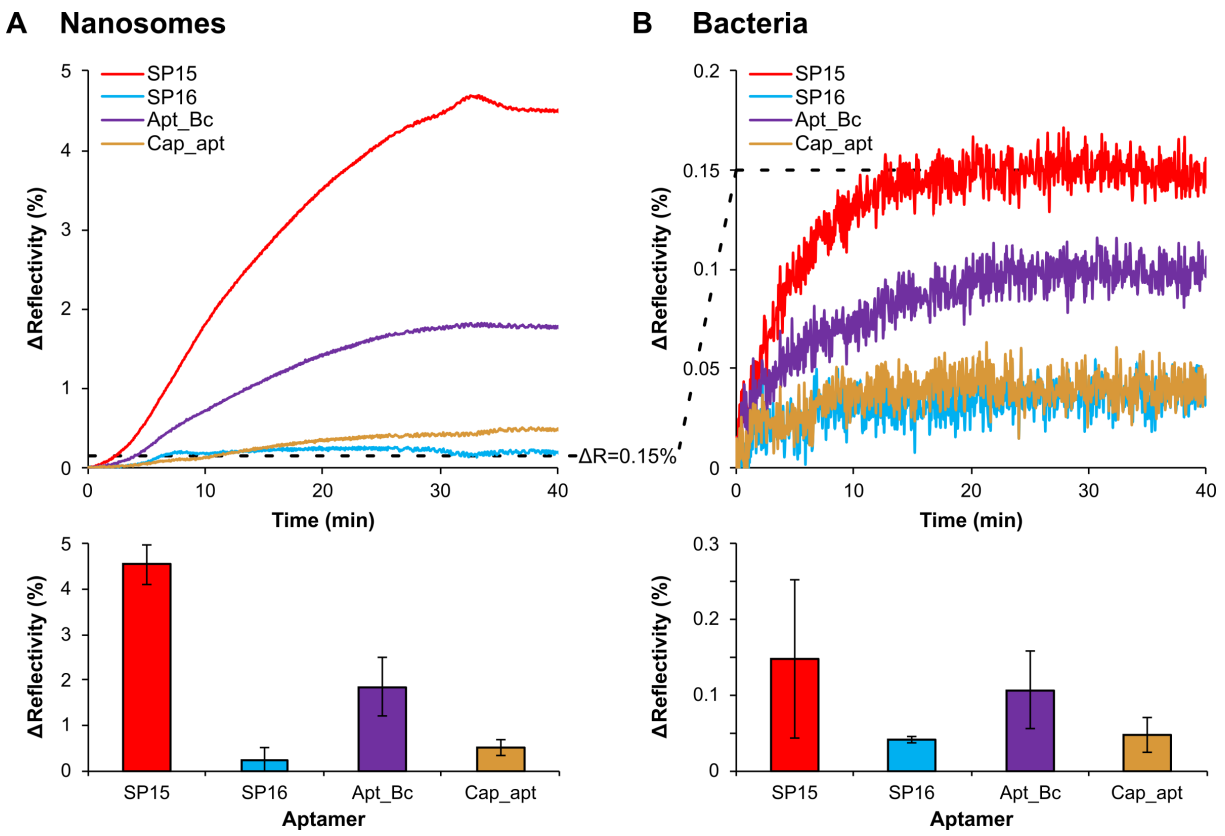

Figure 3. Sensorgrams (top) obtained for the aptamers SP15 (red), Apt_Bc (purple), Cap_apt (gold) and SP16 (blue) during the injection of nanosomes from *B. cereus* grown in BHI at 80 µg/mL protein content (A) or during the injection of *B. cereus* bacteria grown in BHI at a concentration of 3.6 x 10^8 CFU/mL (B). The histograms (bottom) represent points taken from the respective sensorgrams at 40 minutes. The blank signal was subtracted from each sensorgram to eliminate the non-specific signal due to the matrix. Standard errors were taken from five spot replicates.

A binding study was carried out with nanosomes from *B. cereus, B. subtilis* and *E. coli* at a concentration of 80 µg/mL proteins (Figure 4). Nanosomes were injected onto a prism functionalized with the aptamers and the negative control ZIP9. The results showed that the SP15 aptamer is the most sensitive for *B. cereus* nanosomes because it induced the most important shift in the SPR signal. In comparison, the injections of *B. subtilis* and *E. coli* nanosomes induced small shifts in reflectivity, almost identical to those of the control, suggesting a low binding capacity of the nanosomes toward the different aptamers. The SP15 aptamer was therefore retained for the rest of the study.

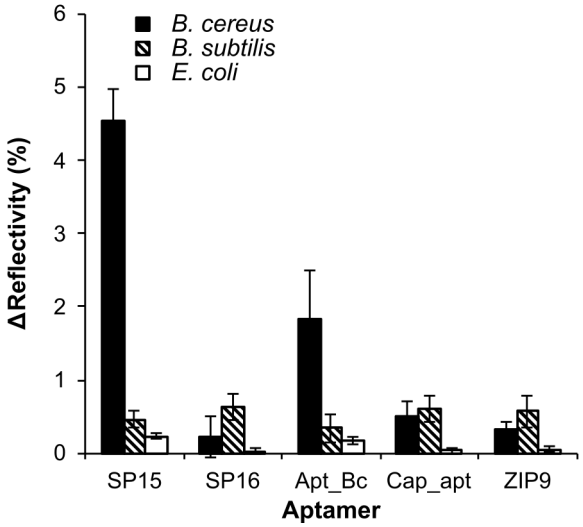

Figure 4. Binding of aptamers (SP15, SP16, Apt_Bc, Capt_apt) and control ZIP9 toward *B. cereus*, *B. subtilis* and *E. coli* nanosomes. The nanosomes were injected at a concentration of 80 µg/mL protein content and the reflectivity shifts were taken from the respective sensorgrams at 40 minutes. The blank signal was subtracted from each sensorgram to eliminate the non-specific signal due to the matrix. Standard errors were calculated from fine spot replicates.

Truncation of the SP15 aptamer. As the SP15 aptamer showed high sensitivity toward *B. cereus* nanosomes, its sequence was truncated to further improve its grafting onto SPRi chips while preserving the specific *B. cereus* binding site. To this end, the two-dimensional conformation of SP15 was modeled using the UNAFold software[21] and its ability to form G-quadruplexes was calculated using the QGRS software,[29] which yielded 28 possible G-quadruplexes (Table S2). The truncations were made assuming that the binding site is located in structural sites of the folded aptamer, such as loops or quadruplexes. Therefore, a medium sequence containing both putative binding sites was selected (SP15M) as well as two short sequences: one containing only the loop site (SP15S1) and the other containing only the G-quadruplex forming unit (SP15S2) (Figure 5).

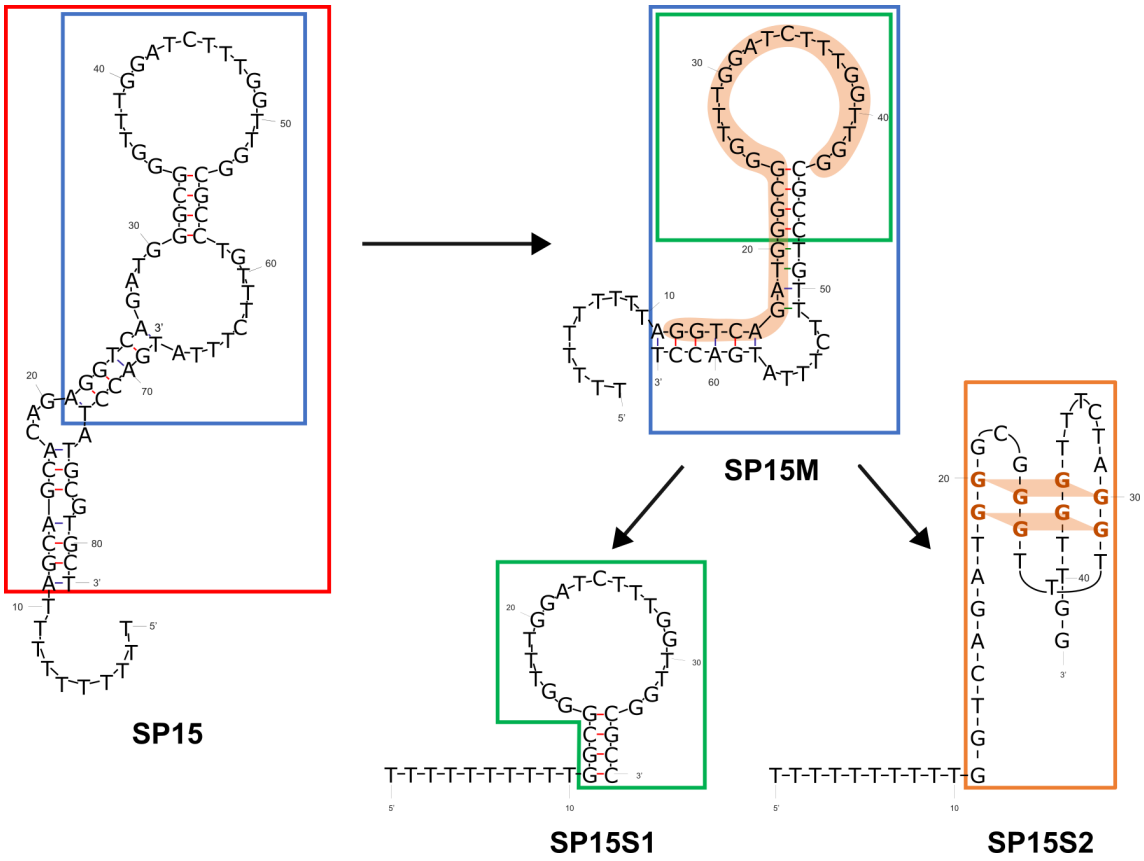

Figure 5. Proposed folded structures for the SP15 aptamer and its truncations.

The melting temperatures (T_m) were approximated using UNAFold software (Table 1).[21] The truncated sequences were only retained if the calculated melting temperature was higher than 40°C. According to the software, the most stable secondary structure for the SP15M truncation, which contains the main loops of SP15, provides an estimated T_m of 63.5°C, so the aptamer would fold properly at room temperature. For its short truncation SP15S1, the sequence retained showed a loop similar to that of SP15 with a predicted T_m of 59.9 °C. Finally, no T_m could be defined for the sequence containing only the G-quadruplex forming unit (SP15S2), since the software does not provide this information.

Apparent association rate constant k_{on} of SP15 truncations. In order to compare the affinity of the SP15 truncations for *B. cereus* nanosomes, cumulative injections were performed with increasing concentrations of nanosome protein content (Figure 6A). The interaction of the nanosomes with the aptamer-functionalized surface induced a strong variation in reflectivity, related to the concentration of nanosomes in solution. Binding of the nanosomes on immobilized

SP15 and SP15M is very similar, suggesting that the sequence allowing *B. cereus* recognition is still present in SP15M. Moreover, all truncations showed some affinity for *B. cereus* nanosomes but shorter structures provided a lower variation of the SPRi signal. This difference between aptamers could be explained by a change in their thermodynamic equilibrium between unfolded and folded structures. The grafting onto SPRi chips could also affect the apparent affinity of the aptamers for their nanosome target.

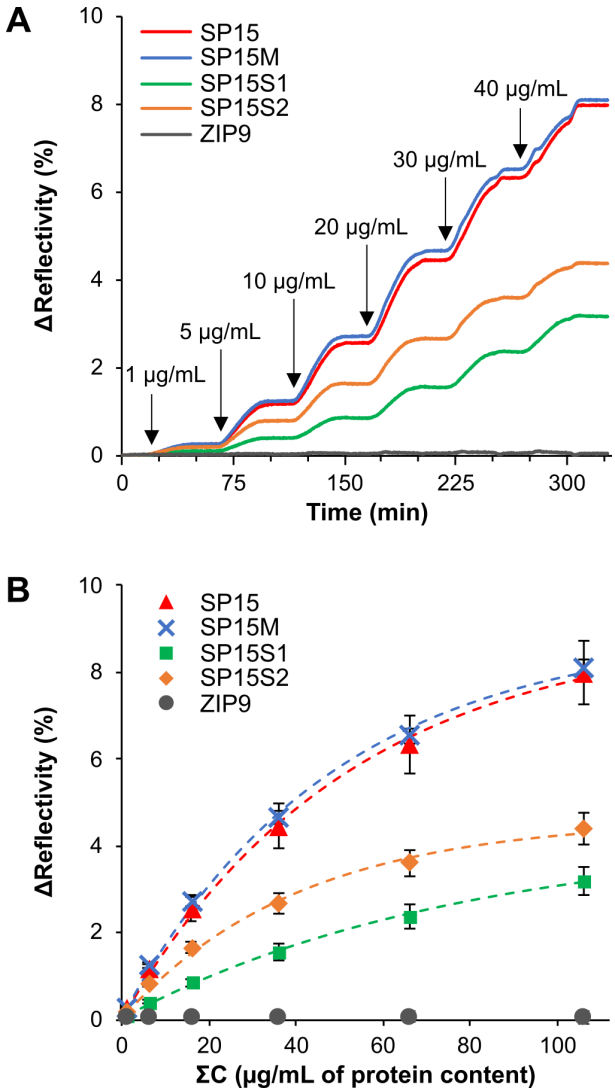

Figure 6. Sensorgrams (A) and kinetic plots ($\Delta R_{plateau}$ vs $\Sigma C_{nanosome}$) (B) obtained for the aptamers SP15 (red), SP15M (blue), SP15S1 (green) and SP15S2 (orange) during the cumulative injections of *B. cereus* grown in BHI nanosomes at 1, 5, 10, 20, 30 and 40 µg/mL protein content. The blank signal was subtracted from each sensorgram to eliminate the non-specific signal due to the matrix. The labels are the $\Delta R_{plateau}$ values corresponding to the reflectivity at the end of each injection (25

min injection time). The dashed lines represent the corresponding fit. Standard errors were calculated from five spot replicates.

In order to compare the affinity of the different truncations for *B. cereus* nanosomes, a kinetic model was developed to fit the data. The Langmuir isotherm model, which follows pseudo-first order kinetics,[30] was used to compare the affinity of the different truncations for *B. cereus* nanosomes. However, this model was slightly modified to correspond to our data. In particular, the dissociation kinetic constant has been removed from the model. Indeed, since a nanosome is likely to contain multiple binding sites for the same aptamers, all the aptamers would have to dissociate simultaneously to release a nanosome in the dissociation state, which is unrealistic. The lack of visible dissociation on the curves is consistent with this statement. It is also assumed that the binding rate is not limited by the mass transfer effect. If this was the case, the binding rate would be greater at higher flow rates. However, experiments at different flow rates showed lower signals at higher flow rates, indicating a slow binding rate of the nanosome to the aptamer.

For all these reasons, pseudo-first-order kinetics are assumed:

$$A + L \xrightarrow{k_{on}} AL$$

where A is the analyte (*B. cereus* binding site), L is the ligand (aptamer), AL the resulting complex and k_{on} the apparent association rate constant. This gives the following rate law:

$$\frac{dR(t)}{dt} = k_{on}.C(t).(R_{max} - R(t)) \qquad (1)$$

where $R(t)$ is reflectivity as a function of time, $C(t)$ is the concentration of nanosomes as a function of time, and R_{max} is the shift in reflectivity corresponding to the maximum amount of nanosomes that can be captured on the aptamer-coated chip surface. By integrating equation (1) between the start and end of an injection, reflectivity can be expressed by the following equation:

$$R_n = R_{max}.\left(1 - \exp\left(-k_{on}.t_{inj}.\sum_{i=0}^{n} C_i\right)\right) \qquad (2)$$

where R_n is the reflectivity at the end of the nth injection, $\sum_{i=0}^{n} C_i$ is the sum of the concentrations of nanosomes injected between the start of the analysis and the nth injection, and t_{inj} is the injection

time, which is equal to 25 minutes. By plotting the reflectivity obtained at each of the six injection ends as a function of the sum of the concentrations of nanosomes injected, the data could be fitted to equation (2) (Figure 6B). The model matches the experimental data as all modeling curves pass through the labels and their standard errors. These curves show a very similar trend for the SP15 aptamer and its SP15M medium truncation. It is also apparent that signal saturation seems to occur more rapidly for SP15S2 than for the other aptamers. This could be explained by a faster association rate of this aptamer with *B. cereus* nanosomes. The fit allowed determination of an apparent association rate constant k_{on} for each aptamer toward *B. cereus* nanosomes and the maximum achievable reflectivity R_{max}. Table 3 summarizes the values calculated for k_{on} and R_{max}, and the R-squared fit for each aptamer.

Table 3. Maximum achievable reflectivity ($\boldsymbol{R_{max}}$) and apparent association rate constant ($\boldsymbol{k_{on}}$) obtained by fitting the SPRi curves of the SP15 aptamer and its truncations. The association rate constant and maximum reflectivity are given as mean ± standard error of the fit.

		SP15	SP15M	SP15S1	SP15S2
ATCC14579 grown in BHI*	R_{max} **(%)**	9.04 ± 0.39	8.97 ± 0.35	4.23 ± 0.30	4.63 ± 0.23
	k_{on} **(L.g^{-1}.s^{-1})**	(1.28 ± 0.11) × 10^{-2}	(1.39 ± 0.12) × 10^{-2}	(8.61 ± 1.02) × 10^{-3}	(1.66 ± 0.19) × 10^{-2}
	R-Square (-)	0.997	0.997	0.997	0.994

*Nanosomes

The fit results for *B. cereus* nanosomes show a slightly higher apparent association rate constant k_{on} for SP15S2 (Table 3), which is the truncation containing only the G-quadruplex forming site. Furthermore, the lower k_{on} is obtained with the SP15S1 truncation containing the loop site. A possible explanation for these results could be that although all truncations appear to contain the binding site necessary for *B. cereus* recognition, the specific conformation caused by the G-quadruplex enhances this recognition. Further studies on SP15S2 would be interesting to investigate the different possible G-quadruplex conformations and to deduce which one is most important for recognition. Another observation is that the maximum amount of nanosomes that can be captured on the aptamer-coated surface, R_{max}, varies according to the aptamers. R_{max} represents the maximum functional ligand for binding on the surface. The shorter aptamer

sequences immobilize a smaller quantity of nanosomes on surface, inducing a lower R_{max}. This observation could be explained by the presence of different conformations on the surface for short aptamers.[31] This reduces the density of well-folded and functional structures.

Binding of aptamer truncations toward *B. cereus*, *B. subtilis* and *E. coli* nanosomes. A binding study of aptamer truncations with nanosomes from *B. cereus*, *B. subtilis* and *E. coli* was carried out (Figure 7). A similar protein concentration of 80 µg/mL was used for the nanosome suspensions.

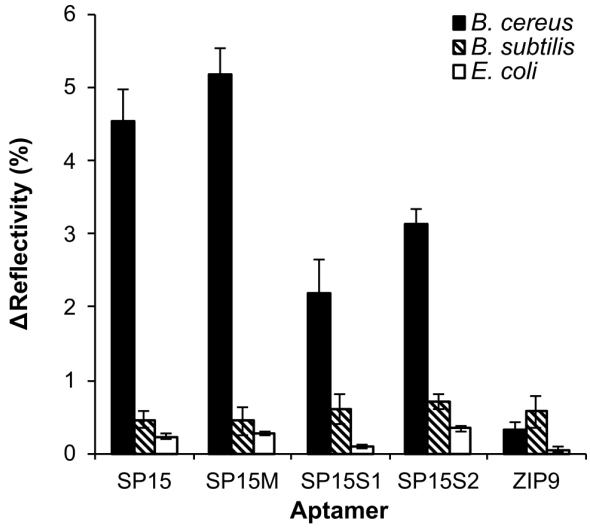

Figure 7. Binding of aptamers and control ZIP9 toward *B. cereus* nanosomes versus *B. subtilis* and *E. coli* nanosomes at 80 µg/mL protein content. The blank signal was subtracted from each bar to eliminate the non-specific signal due to the matrix. The bars are points taken from the respective sensorgrams at 40 minutes of injection. Standard errors were calculated from five spot replicates.

The binding capacities of SP15 truncations toward *E. coli* and *B. subtilis* are low compared to those of *B. cereus*. The results show a higher binding magnitude for the SP15M truncation. Cumulated injections highlighted similar behavior for SP15 and SP15M (Figure 6). Lower binding efficiency is obtained for the short truncations SP15S1 and SP15S2. This could be explained by the fact that the shorter the aptamer, the closer it is to the surface and the more difficult its access, probably due to poor aptamer folding. We also note that the negative control ZIP9 did not provide any significant signal with *B. cereus* nanosomes.

Influence of culture medium and type of strain on the apparent association rate constant k_{on}. *B. cereus* is commonly found in dairy products and the type of growth medium has been shown to

influence the composition of bacterial membrane.[32] Furthermore, aptamer affinity may not be the same for different strains within the wide group of *B. cereus s.s.*.[33] We therefore compared detection of a clinical strain J066 and a commercial strain ATCC14579. Nanosomes from *B. cereus* ATCC14579 grown in milk or *B. cereus* J066 grown in BHI were prepared and characterized (Table S3). Cumulative injections were performed with increasing protein contents of nanosomes from *B. cereus* ATCC14579 grown in milk or *B. cereus* J066, on a biochip functionalized with SP15 truncations (Figure S4). The plot of the reflectivity obtained at each of the six injection ends as a function of the sum of the concentrations of nanosomes injected is presented in Figure 8. The trend is the same as for nanosomes from *B. cereus* ATCC14579 grown in BHI. Indeed, the SP15 aptamer and its medium truncation SP15M gave the higher reflectivity variations. For nanosomes from *B. cereus* ATCC14579 grown in milk, the signals obtained for SP15 and SP15M were quasi-identical. On the other hand, for nanosomes from *B. cereus* J066, it seems that the injected concentrations were not sufficient to reach the R_{max}. As with the nanosomes from *B. cereus* ATCC14579 grown in BHI, the shorter aptamers SP15S1 and SP15S2 provided less variation of the SPRi signal. It is worth noting that for nanosomes from *B. cereus* ATCC14579 grown in milk, maximum reflectivity is reached at around 80 µg/mL of injected protein content, while it is not reached for the other nanosomes even after injection of 106 µg/mL protein content. One possible explanation could be the presence of milk contaminants in the injected solution, altering recognition by forming a surface barrier. The presence of non-specific interactions shown by the slight increase of reflectivity in the ZIP9 signal is consistent with this explanation.

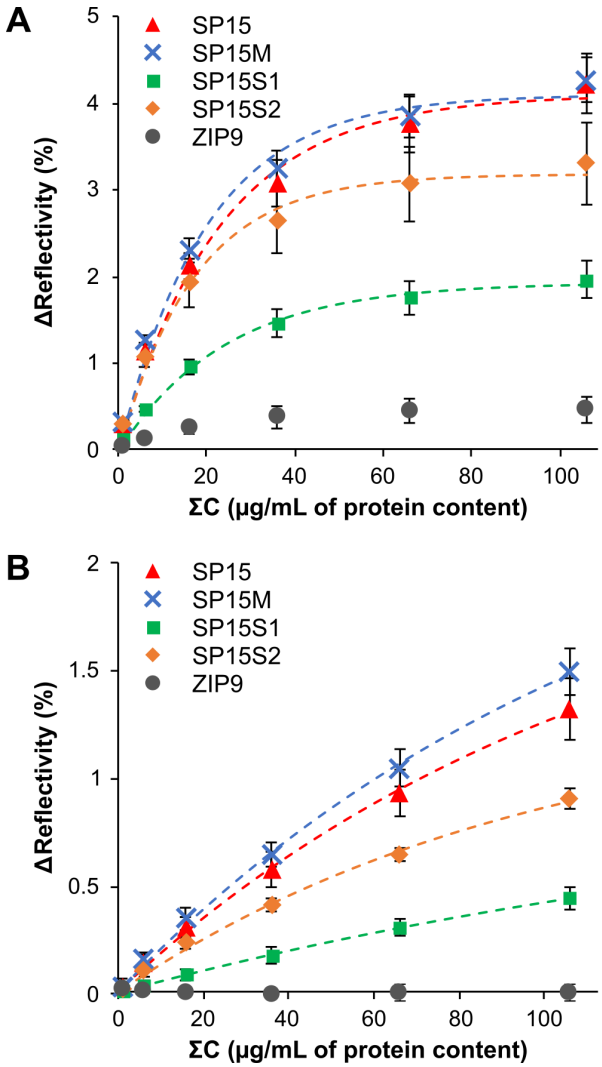

Figure 8. Kinetic plots obtained for the aptamers SP15 (red), SP15M (blue), SP15S1 (green) and SP15S2 (orange) for the cumulative injections of nanosomes from *B. cereus* ATCC14579 grown in milk (A) or from *B. cereus* J066 grown in BHI (B) at 1, 5, 10, 20, 30 and 40 µg/mL protein content. The blank signal was subtracted from each sensorgram to eliminate the non-specific signal due to the matrix. The labels are the $\Delta R_{plateau}$ values corresponding to the reflectivity at the end of each injection (25 min injection time). The dashed lines represent the corresponding fit. Standard errors were calculated from five spot replicates.

Table 4 gives the fit results for nanosomes from *B. cereus* ATCC14579 grown in milk or from *B. cereus* J066 grown in BHI. The apparent association rate constants recorded for *B. cereus* grown in milk (Table 4) revealed to be higher than in BHI (Table 3). A hypothesis to explain this result would be that a residual amount of milk proteins, still present in the medium of the nanosomes after ultracentrifugation, adsorbs non-specifically on the SPRi chip. This adsorption due to contaminants tends to increase the $\Delta R_{plateau}$ and also modify the apparent values of the association rate constants.

Nevertheless, we observe that the order of the association kinetics of the different SP15 truncations is identical to that obtained for the nanosomes grown in BHI. Concerning the results obtained with the clinical strain (J066), the $\Delta R_{plateau}$ and the apparent association kinetic constants are globally smaller than those of the strain ATCC14579, with an apparent association rate constant k_{on} in the order of 10^{-3} L.g^{-1}.s^{-1}, compared with 10^{-2} L.g^{-1}.s^{-1} for other nanosomes. It is known that *B. cereus* group includes numerous strains. Some of them cause foodborne outbreaks in humans.[34] The J066 is a pathogenic strain unlike the strain ATCC14579. Our hypothesis is that a slight difference in surface epitopes influence the association kinetics of aptamers toward nanosomes. The association kinetics were found to be slower for strain J066. However, the association rate constants follow the same trend for both strains J066 and ATTCC14579. These results prove that our approach is suitable for the analysis of clinical strains. For both types of nanosomes, SP15M and SP15S2 exhibit respective association rate constants that best matches the SELEX sequence SP15.

Table 4. Maximum achievable reflectivity ($\boldsymbol{R_{max}}$) and apparent association rate constant ($\boldsymbol{k_{on}}$) obtained by fitting the SPRi curves of the SP15 aptamer and its truncations. The association rate constant and maximum reflectivity are given as mean ± standard error of the fit.

		SP15	SP15M	SP15S1	SP15S2
ATCC14579 grown in milk*	R_{max} **(%)**	4.10 ± 0.16	4.10 ± 0.15	1.93 ± 0.52	3.18 ± 0.10
	k_{on} **(L.g^{-1}.s^{-1})**	(2.91 ± 0.35) × 10^{-2}	(3.36 ± 0.41) × 10^{-2}	(2.76 ± 0.22) × 10^{-2}	(3.87 ± 0.43) × 10^{-2}
	R-Square (-)	0.989	0.988	0.995	0.989
J066 grown in BHI*	R_{max} **(%)**	2.20 ± 0.21	2.54 ± 0.25	1.01 ± 0.06	1.35 ± 0.13
	k_{on} **(L.g^{-1}.s^{-1})**	(5.63 ± 0.78) × 10^{-3}	(5.45 ± 0.75) × 10^{-3}	(3.54 ± 0.26) × 10^{-3}	(6.74 ± 0.10) × 10^{-3}
	R-Square (-)	0.998	0.998	1.000	0.997

*Nanosomes

Proof-of-concept on whole bacteria. The SPRi results showed that *B. cereus* nanosomes have similar association kinetics for the SP15 aptamer and the SP15M truncation. To confirm the binding ability of the selected truncation to the whole *B. cereus* cell, the SP15M aptamer was designed with a fluorescent rhodamine label (Rhod-SP15M) for a microscopic study. After 45 min incubation with 5 x 10^6 CFU/mL of *B. cereus*, the unbound aptamers were removed by centrifugation. The collected pellet was washed once with running buffer, then observed under a fluorescent

microscope on a poly-L-lysine coated slide. A control experiment was carried out using the Rhod-ZIP9 oligonucleotide. The brightfield images in Figure 9 show *B. cereus* bacteria, while the fluorescent field indicates the location of aptamers in the sample. Merging the two images shows that Rhod-SP15M is well distributed on almost all *B. cereus* bacteria (Figure 9C). It demonstrates that Rhod-SP15M binds to *B. cereus* bacteria, imparting fluorescence. However, after incubation of *B. cereus* with Rhod-ZIP9, a large majority of bacteria were not fluorescent (Figure 9F). This indicates that the Rhod-SP15M aptamer binds specifically to *B. cereus*. These results confirm the ability of nanosomes to successfully mimic the bacterial membrane.

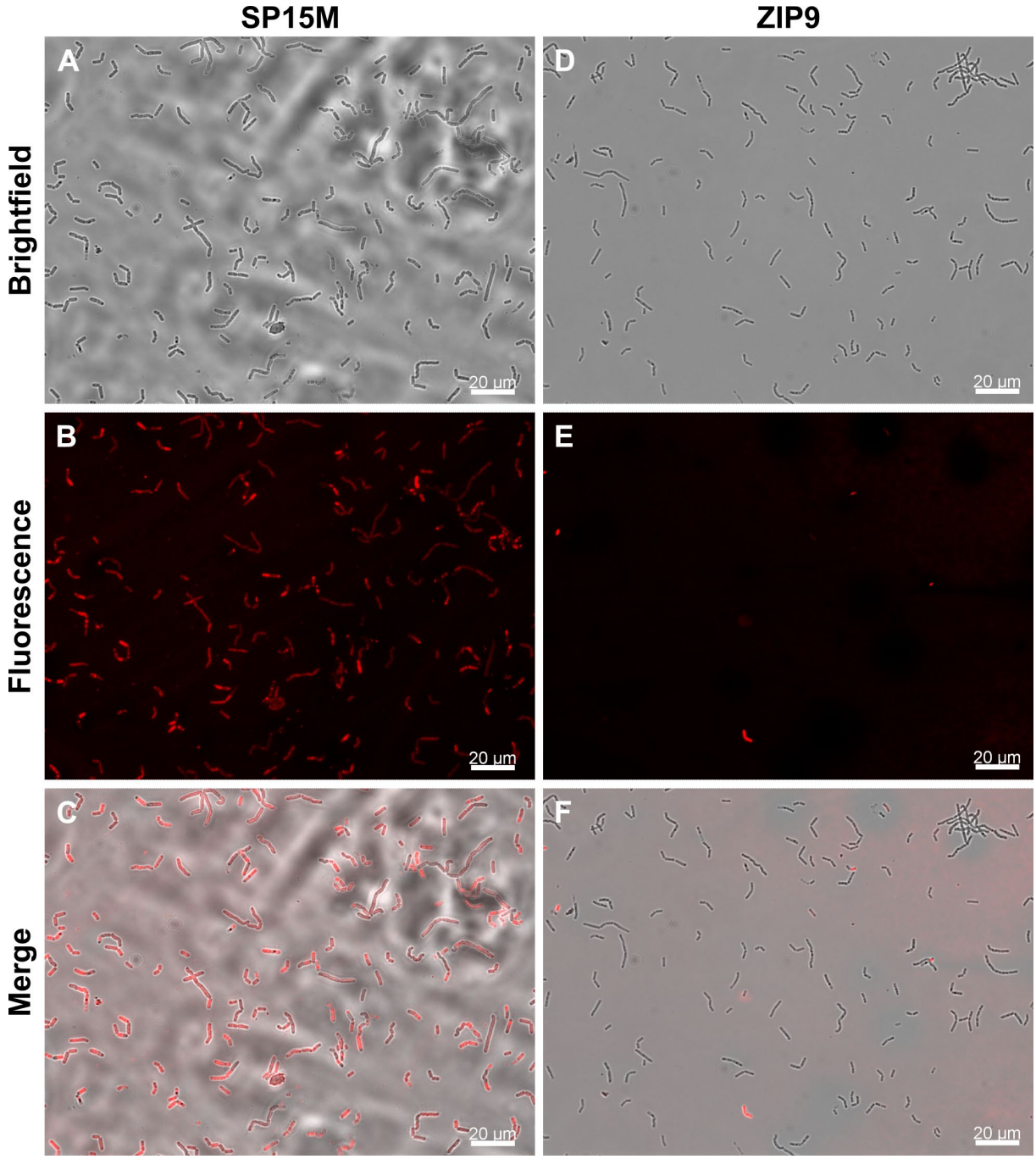

Figure 9. Binding ability of Rhod-SP15M aptamer to *B. cereus* bacteria by fluorescence microscopy (left). Rhod-ZIP9 was used as a nonspecific binding control (right). Images were captured in brightfield without filter (A, D), under fluorescence with a filter set excitation 550/25 nm and emission 605/70 nm (B, E) and merge images (C, F) with a 40x/0.45 objective.

CONCLUSION

A simple method has been developed to compare the affinities of anti-*B. cereus* aptamers and propose new sequences for the subsequent development of a biosensor. Nanosomes have been developed to overcome the problem of SPRi's low sensitivity to large analytes such as bacteria. Characterizations by DLS, NTA, Raman spectroscopy and TEM indicated that nanosomes were formed of lipidic bilayers of vesicular form with diameters ranging in size from 100 to 350 nm. The binding of bacteria and nanosomes onto aptamer-functionalized biochips was studied by SPRi. A 30-fold amplification of the SPRi signal was obtained when *B. cereus* bacterial cells were replaced by their nanosomes. This allowed discrimination among four anti-*B. cereus* aptamers. The SP15 aptamer gave the best signal enhancement. It was also more specific for *B. cereus* nanosomes than for *E. coli* and *B. subtilis* nanosomes. Its sequence was truncated to improve its grafting capacity while preserving the specific *B. cereus* binding site. One medium sequence (SP15M) and two short sequences (SP15S1 and SP15S2) were selected to encourage the formation of either the stem-loop or the G-quadruplex structures. The fit results of SPRi signals for *B. cereus* nanosomes showed a similar trend for the SP15 and SP15M aptamers and a slightly higher apparent association rate constant k_{on} for SP15S2, which is the truncation containing only the G-quadruplex forming site. The same observations were made for the nanosomes from *B. cereus* ATCC14579 grown in milk and the clinical strain *B. cereus* J066. Finally, fluorescence microscopy was used to further confirm the binding of the SP15M aptamer to the whole *B. cereus* cell. This result shows the ability of nanosomes to successfully mimic the bacterial membrane, making it much simpler to compare the affinity of various aptamers toward bacteria with good sensitivity. It is worth noting that nanosomes can also be widely used for screening antibodies, nanobodies or other types of bacterial bioreceptors. This study paves the way for the development of high-performance sensors, facilitated by the easy screening of the best ligands by SPRi.

ASSOCIATED CONTENT

Supporting Information. Raman spectra of *B. cereus* nanosomes (Figure S1), main Raman peak assignments (Table S1), TEM images of *B. cereus* and *E. coli* nanosomes (Figure S2), possible G-quadruplexes for the SP15 aptamer (Table S2), characterization of nanosomes from *B. cereus* ATCC14579 grown in milk and from *B. cereus* J066 grown in BHI (Table S3), sensorgrams obtained for the injection of nanosomes from *B. cereus* ATCC14579 grown in BHI (Figure S3) and sensorgrams obtained for the injection of nanosomes from *B. cereus* ATCC14579 grown in milk and from *B. cereus* J066 grown in BHI (Figure S4).

AUTHOR INFORMATION

Corresponding Authors

*Carole CHAIX: carole.chaix-bauvais@univ-lyon1.fr

*Mathilde MANCEAU: mathilde.manceau@isa-lyon.fr

Author Contributions

The manuscript was written through contributions of all authors. All authors have given approval to the final version of the manuscript.

Funding Sources

This work was supported by the French National Agency for Research (ANR-21-CE21-009 SIENA).

Notes

The authors declare no competing financial interest.

ACKNOWLEDGMENT

The authors thank the French National Agency for Research for financial support of Mathilde Manceau's PhD thesis. They also acknowledge Dr Virginie Rigourd (Région Île-de-France Human Milk Bank, Hôpital Necker-Enfants Malades) for providing us J066 strain, and Majd Khalife (INRAE, France) for technical help.

ABBREVIATIONS

SELEX, systematic evolution of ligands by exponential enrichment; SPR, surface plasmon resonance; SPRi, SPR imaging; BHI, brain heart infusion; T_m, melting temperature; DLS, dynamic light scattering; NTA, nanoparticle tracking analysis; TEM, transmission electron microscopy; ROI, regions of interest; PdI, polydispersity index; SE, standard error; k_{on}, apparent association rate constant; R_{max}, maximum achievable reflectivity; $\Delta R_{plateau}$, reflectivity at the end of injection.

REFERENCES

(1) Ali, M. H.; Elsherbiny, M. E.; Emara, M. Updates on Aptamer Research. *Int. J. Mol. Sci.* **2019**, *20* (10), 2511. https://doi.org/10.3390/ijms20102511.

(2) Su, Y.; Zhu, L.; Wu, Y.; Liu, Z.; Xu, W. Progress and Challenges in Bacterial Whole-Cell-Components Aptamer Advanced Screening and Site Identification. *TrAC Trends Anal. Chem.* **2022**, *157*, 116731. https://doi.org/10.1016/j.trac.2022.116731.

(3) Thevendran, R.; Citartan, M. Assays to Estimate the Binding Affinity of Aptamers. *Talanta* **2022**, *238*, 122971. https://doi.org/10.1016/j.talanta.2021.122971.

(4) Wang, B.; Park, B. Immunoassay Biosensing of Foodborne Pathogens with Surface Plasmon Resonance Imaging: A Review. *J. Agric. Food Chem.* **2020**, *68* (46), 12927–12939. https://doi.org/10.1021/acs.jafc.0c02295.

(5) Foladori, P.; Quaranta, A.; Ziglio, G. Use of Silica Microspheres Having Refractive Index Similar to Bacteria for Conversion of Flow Cytometric Forward Light Scatter into Biovolume. *Water Res.* **2008**, *42* (14), 3757–3766. https://doi.org/10.1016/j.watres.2008.06.026.

(6) Vala, M.; Etheridge, S.; Roach, J. A.; Homola, J. Long-Range Surface Plasmons for Sensitive Detection of Bacterial Analytes. *Sens. Actuators B Chem.* **2009**, *139* (1), 59–63. https://doi.org/10.1016/j.snb.2008.08.029.

(7) Yoo, S. M.; Kim, D.-K.; Lee, S. Y. Aptamer-Functionalized Localized Surface Plasmon Resonance Sensor for the Multiplexed Detection of Different Bacterial Species. *Talanta* **2015**, *132*, 112–117. https://doi.org/10.1016/j.talanta.2014.09.003.

(8) Templier, V.; Livache, T.; Boisset, S.; Maurin, M.; Slimani, S.; Mathey, R.; Roupioz, Y. Biochips for Direct Detection and Identification of Bacteria in Blood Culture-Like Conditions. *Sci. Rep.* **2017**, *7* (1), 9457. https://doi.org/10.1038/s41598-017-10072-z.

(9) Belkilani, M.; Shokouhi, M.; Farre, C.; Chevalier, Y.; Minot, S.; Bessueille, F.; Abdelghani, A.; Jaffrezic-Renault, N.; Chaix, C. Surface Plasmon Resonance Monitoring of Mono-Rhamnolipid Interaction with Phospholipid-Based Liposomes. *Langmuir* **2021**, *37* (26), 7975–7985. https://doi.org/10.1021/acs.langmuir.1c00846.

(10) Belkilani, M.; Farre, C.; Chevalier, Y.; Minot, S.; Bessueille, F.; Abdelghani, A.; Jaffrezic-Renault, N.; Chaix, C. Mechanisms of Influenza Virus HA2 Peptide Interaction with Liposomes Studied by Dual-Wavelength MP-SPR. *ACS Appl. Mater. Interfaces* **2022**, *14* (29), 32970–32981. https://doi.org/10.1021/acsami.2c09039.

(11) Toyofuku, M.; Nomura, N.; Eberl, L. Types and Origins of Bacterial Membrane Vesicles. *Nat. Rev. Microbiol.* **2019**, *17* (1), 13–24. https://doi.org/10.1038/s41579-018-0112-2.

(12) Cao, Y.; Lin, H. Characterization and Function of Membrane Vesicles in Gram-Positive Bacteria. *Appl. Microbiol. Biotechnol.* **2021**, *105* (5), 1795–1801. https://doi.org/10.1007/s00253-021-11140-1.
(13) Elie-Caille, C.; Fliniaux, O.; Pantigny, J.; Mazière, J.-C.; Bourdillon, C. Self-Assembly of Solid-Supported Membranes Using a Triggered Fusion of Phospholipid-Enriched Proteoliposomes Prepared from the Inner Mitochondrial Membrane1. *Langmuir* **2005**, *21* (10), 4661–4668. https://doi.org/10.1021/la046973k.
(14) Minic Vidic, J.; Grosclaude, J.; Persuy, M.-A.; Aioun, J.; Salesse, R.; Pajot-Augy, E. Quantitative Assessment of Olfactory Receptors Activity in Immobilized Nanosomes: A Novel Concept for Bioelectronic Nose. *Lab. Chip* **2006**, *6* (8), 1026–1032. https://doi.org/10.1039/B603189G.
(15) Tallent, S. M.; Knolhoff, A.; Rhodehamel, E. J.; Harmon, S. M.; Bennett, R. W. BAM Chapter 14: Bacillus Cereus. In *Bacteriological Analytical Manual*; United States Food and Drug Administration, Ed.; AOAC International, 1998.
(16) Glasset, B.; Herbin, S.; Guillier, L.; Cadel-Six, S.; Vignaud, M.-L.; Grout, J.; Pairaud, S.; Michel, V.; Hennekinne, J.-A.; Ramarao, N.; Brisabois, A. Bacillus Cereus-Induced Food-Borne Outbreaks in France, 2007 to 2014: Epidemiology and Genetic Characterisation. *Eurosurveillance* **2016**, *21* (48), 30413. https://doi.org/10.2807/1560-7917.ES.2016.21.48.30413.
(17) Authority, E. F. S.; European Centre for Disease Prevention and Control. The European Union One Health 2019 Zoonoses Report. *EFSA J.* **2021**, *19* (2), e06406. https://doi.org/10.2903/j.efsa.2021.6406.
(18) Wang, Z.; Yang, H.; Xia, Y.; Duan, N. Oligonucleotide Aptamer Set for Specifically Identifying Bacillus Cereus. CN104694646A, 2015.
(19) Zhou, Z.; Lan, X.; Zhu, L.; Zhang, Y.; Chen, K.; Zhang, W.; Xu, W. Portable Dual-Aptamer Microfluidic Chip Biosensor for Bacillus Cereus Based on Aptamer Tailoring and Dumbbell-Shaped Probes. *J. Hazard. Mater.* **2023**, *445*, 130545. https://doi.org/10.1016/j.jhazmat.2022.130545.
(20) Zheng, H.; Sheng, R.; Li, H.; ahmad, W.; Chen, Q. Rapid and Selective Detection of Bacillus Cereus in Food Using cDNA-Based up-Conversion Fluorescence Spectrum Copy and Aptamer Modified Magnetic Separation. *Spectrochim. Acta. A. Mol. Biomol. Spectrosc.* **2022**, *267*, 120618. https://doi.org/10.1016/j.saa.2021.120618.
(21) *DNA Folding Form*. http://www.unafold.org/mfold/applications/dna-folding-form.php (accessed 2023-09-13).
(22) Vidic, J.; Hou, Y. Immobilization of Olfactory Receptors Carried by Nanosomes onto a Gold Sensor Surface. *G Protein-Coupled Recept. Screen. Assays Methods Protoc.* **2021**, 85–95. https://doi.org/10.1007/978-1-0716-1221-7_6.
(23) Danaei, M.; Dehghankhold, M.; Ataei, S.; Hasanzadeh Davarani, F.; Javanmard, R.; Dokhani, A.; Khorasani, S.; Mozafari, M. R. Impact of Particle Size and Polydispersity Index on the Clinical Applications of Lipidic Nanocarrier Systems. *Pharmaceutics* **2018**, *10* (2), 57. https://doi.org/10.3390/pharmaceutics10020057.
(24) Kurbangaleeva, S. V.; Syromiatnikova, V. Y.; Prokopeva, A. E.; Rogov, A. M.; Khannanov, A. A.; Rizvanov, A. A.; Gomzikova, M. O. Increased Yield of Extracellular Vesicles after Cytochalasin B Treatment and Vortexing. *Curr. Issues Mol. Biol.* **2023**, *45* (3), 2431–2443. https://doi.org/10.3390/cimb45030158.
(25) Tiwari, S.; Kumar, V.; Randhawa, S.; Verma, S. K. Preparation and Characterization of Extracellular Vesicles. *Am. J. Reprod. Immunol.* **2021**, *85* (2), e13367. https://doi.org/10.1111/aji.13367.
(26) Su, Y.; Zhu, L.; Wu, Y.; Liu, Z.; Xu, W. Progress and Challenges in Bacterial Whole-Cell-Components Aptamer Advanced Screening and Site Identification. *TrAC Trends Anal. Chem.* **2022**, *157*, 116731. https://doi.org/10.1016/j.trac.2022.116731.

(27) Vidic, J.; Pla-Roca, M.; Grosclaude, J.; Persuy, M.-A.; Monnerie, R.; Caballero, D.; Errachid, A.; Hou, Y.; Jaffrezic-Renault, N.; Salesse, R.; Pajot-Augy, E.; Samitier, J. Gold Surface Functionalization and Patterning for Specific Immobilization of Olfactory Receptors Carried by Nanosomes. *Anal. Chem.* **2007**, *79* (9), 3280–3290. https://doi.org/10.1021/ac061774m.
(28) Martin, J. A.; Chushak, Y.; Chávez, J. L.; Hagen, J. A.; Kelley-Loughnane, N. Microarrays as Model Biosensor Platforms to Investigate the Structure and Affinity of Aptamers. *J. Nucleic Acids* **2016**, *2016*, e9718612. https://doi.org/10.1155/2016/9718612.
(29) *QGRS Mapper | Analyze and Search*. https://bioinformatics.ramapo.edu/QGRS/analyze.php (accessed 2023-09-13).
(30) Halperin, A.; Buhot, A.; Zhulina, E. B. On the Hybridization Isotherms of DNA Microarrays: The Langmuir Model and Its Extensions. *J. Phys. Condens. Matter* **2006**, *18* (18), S463. https://doi.org/10.1088/0953-8984/18/18/S01.
(31) Schasfoort, R. B. M. Introduction to Surface Plasmon Resonance. In *Handbook of Surface Plasmon Resonance*; Schasfoort, R. B. M., Ed.; The Royal Society of Chemistry, 2017; pp 1–16. https://doi.org/10.1039/9781788010283-00001.
(32) Murakami, Y.; Imai, M.; Mukai, Y.; Ichihara, S.; Nakamura, H.; Yoshimura, F. Effects of Various Culture Environments on Expression of Major Outer Membrane Proteins from Porphyromonas Gingivalis. *FEMS Microbiol. Lett.* **2004**, *230* (2), 159–165. https://doi.org/10.1016/S0378-1097(03)00896-6.
(33) Fischer, C.; Hünniger, T.; Jarck, J.-H.; Frohnmeyer, E.; Kallinich, C.; Haase, I.; Hahn, U.; Fischer, M. Food Sensing: Aptamer-Based Trapping of Bacillus Cereus Spores with Specific Detection via Real Time PCR in Milk. *J. Agric. Food Chem.* **2015**, *63* (36), 8050–8057. https://doi.org/10.1021/acs.jafc.5b03738.
(34) Vidic, J.; Chaix, C.; Manzano, M.; Heyndrickx, M. Food Sensing: Detection of Bacillus Cereus Spores in Dairy Products. *Biosensors* **2020**, *10* (3), 15. https://doi.org/10.3390/bios10030015.

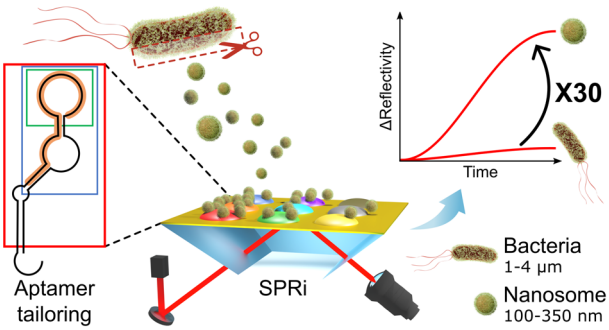

For Table of Contents Only